Journal of Iron and Steel Research, International 24 (2017) 1248—1253

Contents lists available at ScienceDirect

Journal of Iron and Steel Research, International

journal homepage: www.chinamet.cn

Effect of heat input on microstructure and mechanical properties of dissimilar joints of AISI 316L steel and API X70 high-strength low-alloy steel

Ebrahim Mortazavi, Reza Amini Najafabadi, Amirhossein Meysami*

Metallurgy & Materials Department, Golpayegan University of Technology, Golpayegan 65651, Iran

ARTICLE INFO

Key words:
Dissimilar joint
AISI 316L steel
API X70 high-strength low-alloy steel
Transition region
Heat input

ABSTRACT

The microstructure and mechanical properties of dissimilar joints of AISI 316L austenitic stainless steel and API X70 high-strength low-alloy steel were investigated. For this purpose, gas tungsten arc welding (GTAW) was used in three different heat inputs, including 0.73, 0.84, and 0.97 kJ/mm. The microstructural investigations of different zones including base metals, weld metal, heat-affected zones and interfaces were performed by optical microscopy and scanning electron microscopy. The mechanical properties were measured by microhardness, tensile and impact tests. It was found that with increasing heat input, the dendrite size and inter-dendritic spacing in the weld metal increased. Also, the amount of delta ferrite in the weld metal was reduced. Therefore, tensile strength and hardness were reduced and impact test energy was increased. The investigation of the interface between AISI 316L base metal and ER316L filler metal showed that increasing the heat input increases the size of austenite grains in the fusion boundary. A transition region was formed at the interface between API X70 steel and filler metals.

1. Introduction

Stainless steels are among the most extensively used special alloys that have been developed against corrosion. Austenitic stainless steels are the biggest group of stainless steels, and grades of AISI 316 and AISI 304 steel are the most commonly used austenitic stainless steels. These steels are generally considered to be very weldable. On the other hand, problems such as hot cracking and sensitization phenomena occur in these steels' weld metal and heat-affected zone. In order to solve these problems, a very low carbon grade like 316L and 304L has commonly been used[1,2].

High-strength low-alloy (HSLA) steels are used extensively in oil and gas pipelines. Achieving high transmission efficiency becomes possible by constructing transmission pipelines using high-strength steels, which allow for high operating pressures and high rates of transmission. Owing to the economic benefits as well as the full advantage of the outstanding performance of two metals, such as strength and corrosion resistance, dissimilar welding is used extensively in the oil and gas industries[3,4].

Some researchers have focused on the properties of dissimilar welding, and a significant amount of research work has been carried out on the welding behavior and mechanical properties of dissimilar welding joints[5-7]. Generally, the joining of dissimilar steels is more challenging than that of similar steels on account of several factors, such as the differences in chemical compositions and thermal expansion coefficients, which lead to different residual stress situations across the different regions of weldments as well as the migration of carbon elements from the steel with higher carbon content to the steel with relatively lower carbon content[8-12]. Gas tungsten arc welding (GTAW) is widely employed in joining processes, especially in those dealing with structural and piping applications.

Lin and Hsieh[13] studied the effect of Si content for 309L filler metal on the dissimilar welding of AISI 1017 and AISI 304L steels. The result showed that Si can increase the formation of δ-ferrite and the sigma phase in the weld metal.

Arivazhagan et al.[14] investigated the effect of heat input on the microstructure and mechanical properties of dissimilar welding of 304 austenitic stainless steel and 4140 low alloy steel. It was found that as heat input increases, the micro-segregation

* Corresponding author. Assist. Prof., Ph.D.
E-mail address: *meysami@gut.ac.ir* (*A. Meysami*).

Received 11 November 2016; Received in revised form 16 May 2017; Accepted 17 May 2017
Available online 15 December 2017

of alloying elements increases, and also creates a chromium depletion zone in the grain boundaries; therefore, the mechanical properties of the joints are determinate.

Sadeghian et al.[15] studied the effect of heat input on the microstructure and mechanical properties of a dissimilar welding joint of super-duplex stainless steel and high-strength low-alloy steel by gas tungsten arc welding. Results indicated that an increase in heat input leads to a decrease in ferrite percentage. Besides, there were no harmful secondary phases, neither carbides nor nitrides. It also indicated the bainite and ferrite phases formed in the heat-affected zone of HSLA base metal in low heat input. However, in high heat input, pearlite and ferrite phases formed.

Ramkumar et al.[16] investigated the microstructure and mechanical properties of dissimilar UNS 32750/AISI 316L welded joint. They reported that microstructure studies revealed the presence of ferrite at the heat-affected zone of AISI316L and the fusion zone obviated the hot cracking tendency. Also, tensile studies showed that the strength of joint was sufficiently greater than that of parent metals and the impact toughness was slightly poor, due to the presence of large platelets of Widmanstatten ferrite in the fusion zone.

The present work evaluates the effect of heat input on the microstructural development and the mechanical properties of dissimilar AISI 316L/API X70 steel joints prepared by GTAW.

2. Experimental Procedure

AISI 316L austenitic stainless steel and API X70 high-strength low-alloy steel were welded together in dimensions of 100 mm×70 mm×10 mm (Fig. 1) by GTAW. A 70-degree single V groove edge with a root face gap of 2 mm was employed before welding. Also, an ER316L welding rod was used and the welding was carried out in five passes to join AISI 316L to API X70 HSLA steel. The chemical compositions of base metals and filler metal are shown in Table 1, and welding parameters are shown in Table 2.

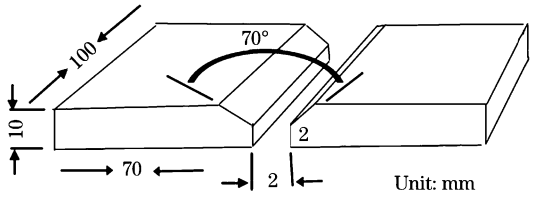

Fig. 1. Design of weldment.

Table 1
Chemical compositions of base metals and filler metals (wt.%)

Component	C	Si	Mn	P	S	Ni	Cr	Cu	Mo	Ti	Nb	Al
API X70	0.09	0.45	0.90	0.04	≤0.020	0.4	0.25	—	0.08	0.010	0.050	0.0300
AISI 316L	0.06	0.47	1.38	0.01	≤0.005	13.0	17.00	0.058	2.00	0.002	0.009	0.0036
ER316L	0.03	0.90	1.73	0.03	≤0.030	11.5	19.30	0.700	2.50	—	—	—

Table 2
Welding parameters

Current/A	Voltage/V	Speed/(mm·s^{-1})	Heat input/(kJ·mm^{-1})
160	13	1.69	0.73
180	14	1.78	0.84
200	15	1.85	0.97

Ferrite number measurement was also carried out by using Ferritescope FMP30 produced in Russia. The results of the Ferritescope are listed in Table 3.

In order to evaluate the mechanical properties, tensile test according to ASTM E8 standard, impact test according to ASTM E23 standard and microhardness test according to ASTM E384 were performed. After the tensile test and impact test, all the fracture surfaces of the specimens were examined by using a field emission scanning electron microscope (FESEM). A microhardness test with force loading of 0.98 N for 10 s was conducted across the base metals, heat-affected zones and weld metals. The notch impact test specimens with dimensions of 55 mm×10 mm×10 mm and 2 mm notches with an angle of 45° were prepared, and the tests were conducted at room temperature and －5 ℃. The weld metal was placed at the centers of the specimens. The Charpy impact test was performed on the specimen at room temperature.

Table 3
Result of Ferritescope

Heat input/(kJ·mm^{-1})	Ferrite/%	Austenite/%
0.73	5.2	94.8
0.84	3.3	96.7
0.97	2.1	97.9

Metallographic observation was carried out to study the microstructures of base metals, weld metal, heat-affected zones and microstructural changes. The specimens of API X70 steel were etched in nital (2 vol. % nitrate acid in alcohol) for 20 s; specimens of AISI 316L austenitic stainless steel were electro-etched in 60 vol. % nitric acid at 5 V for 60 s and specimens of austenitic stainless steel weld metal were etched by Marble's reagent (10 g $CuSO_4$ +50 mL

HCl+50 mL H_2O) for 20 s.

3. Results and Discussion

3.1. Base metal microstructure

The microstructures of AISI 316L austenitic stainless steel and API X70 HSLA steel are respectively displayed in Figs. 2(a) and 2(b). Austenite grains are seen in the microstructure of base metal while the microstructure of API X70 HSLA steel reveals a mixture of ferrite and pearlite.

3.2. Weld metal microstructure

The microstructure of ER316L filler metal is shown in Fig. 3. As can be seen, the microstructure of ER316L weld metal consists of skeletal ferrite in austenitic matrix. The solidification mode was ferrite-austenite in this weld. In this mode, ferrite is the primary solidified phase (proeutectic phase) and austenite is formed at lower temperature by a eutectic reaction.

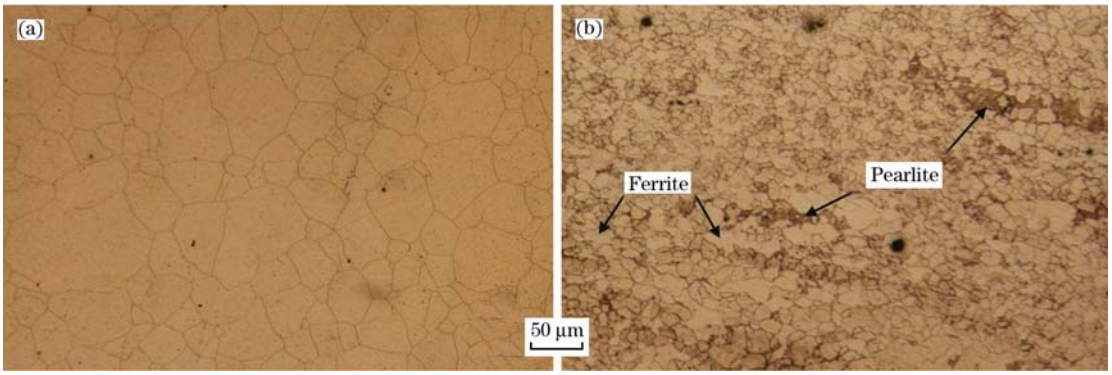

Fig. 2. Microstructure of AISI 316L austenitic stainless steel base metal (a) and microstructure of API X70 high strength low alloy steel base metal (b).

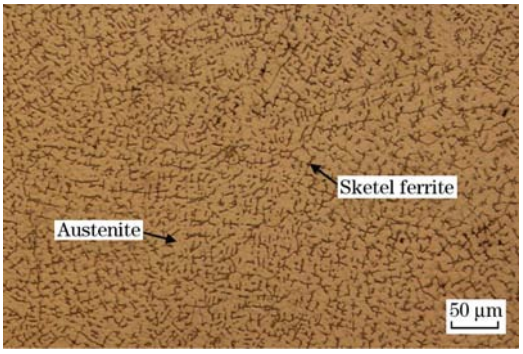

Fig. 3. Microstructure of ER316L austenitic weld metal.

Heat input has a direct influence on the cooling rate. The cooling rate decreases with increasing heat input and the austenite-ferrite transformation will further develop under the ferrite dissolution line in Fe-C diagram[9,10]. Fig. 4(a－c) shows the effect of heat input on the microstructure of ER316L weld metal. According to the Ferritescope results (listed in Table 3), it is found that with increase in heat input, the amount of δ-ferrite has been reduced in weld metal. In other words, when heat input increases, the dendrite size and inter-dendritic spacing in the weld metal also increase.

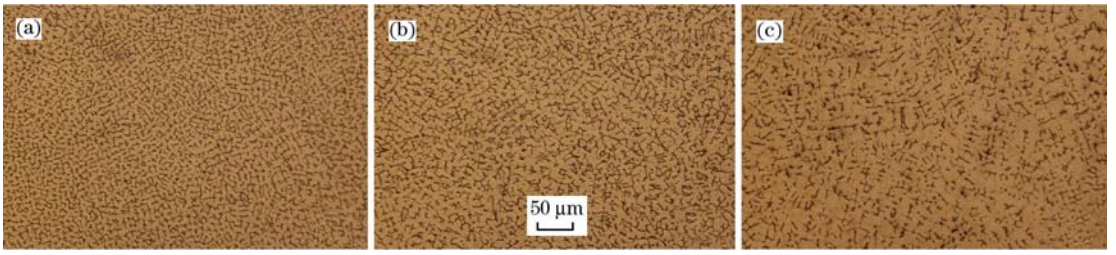

(a) 0.73 kJ/mm; (b) 0.84 kJ/mm; (c) 0.97 kJ/mm.

Fig. 4. Microstructures of ER316L weld metal with different heat inputs.

3.3. Interfacial microstructures

3.3.1. Interface of AISI 316L base metal and ER316L weld metal

The interface of ER316L weld metal and AISI 316L base metals is shown in Fig. 5. As these images show, the interface between weld metal and 316L base metal is completely joined, and no transition region, unmixed zone and crack are seen. Epitaxial growth in interface of AISI 316L base metal and ER316L filler metal is obviously seen.

The effect of heat input on the interface between weld metal and AISI 316L base metal has been shown

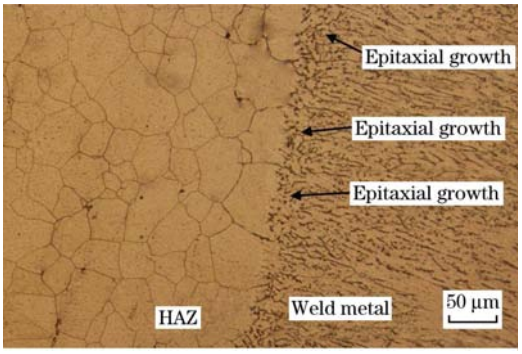

Fig. 5. Interface between AISI 316L base metal and ER316L weld metal.

in Fig. 6. Optical microscopy observation indicated that the austenitic grain adjacent to fusion line coarsens with increasing heat input, and thus increasing heat input causes an increase in the heat-affected zone.

3.3.2. Interface of API X70 base metal and ER316L weld metal

The interface of ER316L weld metal and API X70 base metal is shown in Fig. 7. The obvious phenomenon seen in this figure is the existence of a delicate transition region in the fusion boundary between weld metal and base metal. The transition region can be the result of differences in the crystal structures of weld metal and base metal, density gradient in fusion

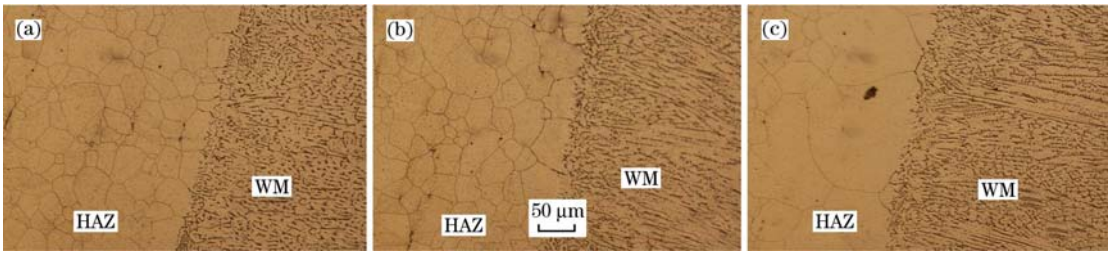

(a) 0.73 kJ/mm; (b) 0.84 kJ/mm; (c) 0.97 kJ/mm.

Fig. 6. Interface between AISI 316L base metal and ER316L weld metal with different heat inputs.

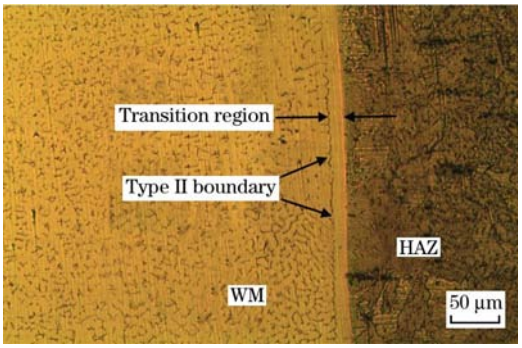

Fig. 7. Interface between API X70 base metal and ER316L weld metal.

boundary, and growth kinetics in welding. This is the structural change of Type II boundary, which was composed along the fusion boundary[17,18].

The effect of heat input on interface between ER316L weld metal and API X70 base metal is shown in Fig. 8(a－c). It is observed that as the heat input increases, the width of the transition region also increases to a limited extent. By increasing heat input Type II, the migration of the borders increases toward weld metal.

3.4. Mechanical properties

3.4.1. Tensile test

The tensile results are listed in Table 4. The tensile

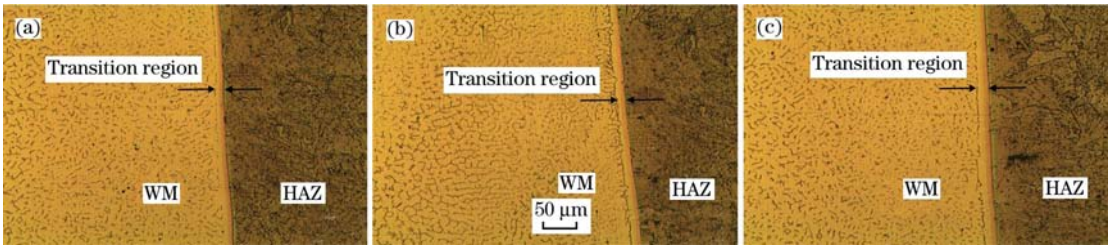

(a) 0.73 kJ/mm; (b) 0.84 kJ/mm; (c) 0.97 kJ/mm.

Fig. 8. Interface between AISI 316L base metal and ER316L weld metal with different heat inputs.

results show that the maximum tensile strength of 544 MPa is related to the specimen welded using low heat input, and minimum tensile strength of 536 MPa is related to the specimen welded using high heat input. Because of the increase in heat input and the results of the Ferritescope (Table 3), it is observed that by reducing weld metal ferrite content, the strength at room temperature is increased[19,20].

The fractured surfaces of the tensile specimen were analyzed using SEM and the fracture locations belong

Table 4
Results of tensile test

Heat input/ (kJ · mm^{-1})	Elongation/ %	Ultimate stress/MPa	Yield stress/MPa
0.73	45.1	544	359
0.84	47.2	541	354
0.97	49.6	536	349

to weldment. Fig. 9 shows the SEM fractographs of the joints after tensile test. Dimples were observed in all the fractured surfaces, indicating that the fractured mechanism is ductile[11]. From Fig. 9(a－c), it is observed that as the heat input increases, coarse and elongated dimples are observed.

3.4.2. Notch impact test

The effect of the heat input on impact energy is shown in Fig. 10. The notch location in specimens was designed in the weldment. It is observed that as heat input increases, the impact energy of the specimen also increases. Because of the results of the Ferritescope which are listed in Table 3, it is found that by increasing weld metal austenite content, impact energy increased, since the presence of austenite tends to increase toughness[21,22].

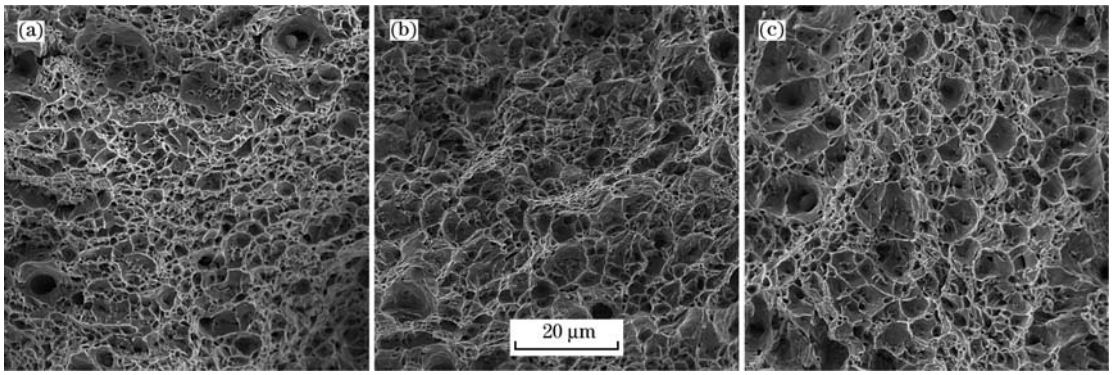

(a) 0.73 kJ/mm; (b) 0.84 kJ/mm; (c) 0.97 kJ/mm.
Fig. 9. SEM fractographs of joints tensile tested with different heat inputs.

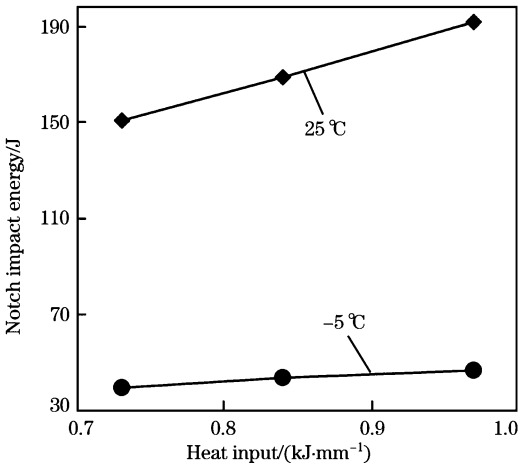

Fig. 10. Results of notch impact test.

The fractured surfaces of the impact specimen were analyzed using SEM. Fig. 11 shows the SEM fractographs of the joint regions. Dimples were observed in all the fractured surfaces, which indicate that the fractured mechanism is ductile. From Fig. 11(a－c), it is clarified that as heat input increases, coarse and elongated dimples are observed.

3.4.3. Microhardness profile

The effects of heat input on microhardness of weldments are shown by Fig. 12. It is observed that as heat input increases, the hardness of the weld metal decreases. From the results of the Ferritescope listed

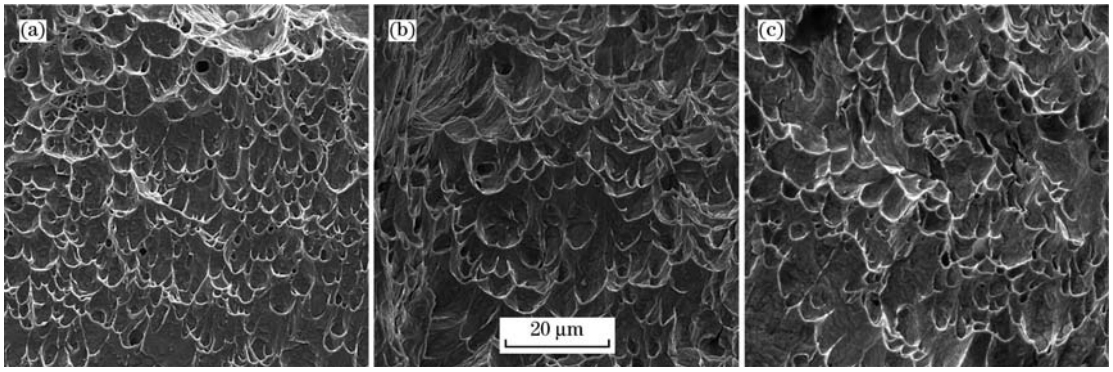

Fig. 11. SEM fractographs of joints impact tested with low heat input (a), normal heat input (b) and high heat input (c).

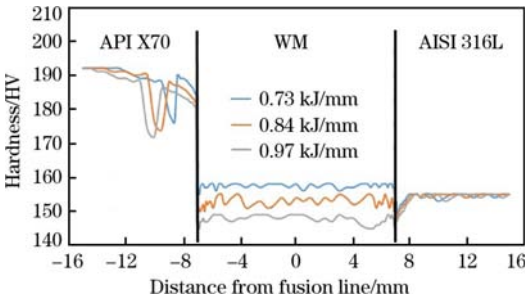

Fig. 12. Microhardness profiles of dissimilar metal welding with different heat inputs.

in Table 3, it is observed that a reduction in the weld metal ferrite content leads to a decrease in hardness. Also, increased heat input causes an increase in the width of both the base metal HAZ.

4. Conclusions

(1) The interface between weld metal and 316L base metal is completely joined. Epitaxial growth in interface of AISI 316L base metal and ER316L base metal was observed.

(2) The Type II boundary and transition region in the fusion boundary between weld metal and X70 steel base metal were observed.

(3) With increasing heat input, the amount of δ-ferrite has been reduced in weld metal. Also, the dendrite size and inter-dendritic spacing in the weld metal increase.

(4) With increases in the heat input, the amount of ferrite in the weld metal is reduced. Therefore, with increasing heat input, tensile strength and hardness decrease, and impact energy increases.

References

[1] J. C. Lipold, D. Kotecki, Welding Metallurgy and Weldability of Stainless Steels, Wiley, New York, 2005.
[2] P. D. Teidra, O. Martin, Mater. Des. 49 (2013) 103-110.
[3] S. H. Hashemi, D. Mohammadyani, M. Pouranvari, S. M. Mousavizadeh, Eng. Mater. 32 (2009) 33-39.
[4] L. Zhongqiu, F. Jian, Z. Yong, Y. Zexi, Energy Proc. 16 (2012) 444-450.
[5] M. K. Samal, M. Seidenfuss, E. Roos, K. Balani, Eng. Fail. Anal. 18 (2011) 993-999.
[6] G. Phanikumar, K. Chattopadhyay, P. Dutta, Sci. Technol. Weld. Join. 16 (2011) 306-313.
[7] H. Naffakh, M. Shamanian, F. Ashrafizadeh, J. Mater. Process. Technol. 209 (2009) 3623-3628.
[8] M. M. A. Khana, L. Romolia, M. Fiaschib, G. Dinia, F. Sarri, J. Mater. Process. Technol. 212 (2012) 856-862.
[9] S. Wang, Q. Ma, Y. Li, Mater. Des. 32 (2011) 831-839.
[10] C. H. Lee, K. H. Chang, J. Mater. Sci. 42 (2007) 6607-6614.
[11] P. Sedeka, J. Brozda, L. Wang, P. J. Withers, Int. J. Press. Vessels Pip. 80 (2003) 705-711.
[12] E. Ranjbarnodeh, S. Serajzadeh, A. H. Kokabi, S. Hanke, A. Fischer, Int. J. Adv. Manuf. Technol. 55 (2011) 649-656.
[13] D. Y. Lin, C. C. Hsieh, Met. Mater. Int. 15 (2009) 507-514.
[14] N. Arivazhagan, S. Singh, S. Prakash, G. M. Reddy, Mater. Des. 32 (2011) 3036-3042.
[15] M. Sadeghian, M. Shamanian, A. Shafyei, Mater. Des. 60 (2014) 678-684.
[16] K. D. Ramkumar, A. Bajpai, S. Raghuvanshi, Mater. Sci. Eng. A 638 (2015) 60-66.
[17] B. Mvola, P. Kah, J. Martikainen, R. Suoranta, Rev. Adv. Mater. Sci. 44 (2016) 146-159.
[18] M. Al Hajri, A. U. Malik, A. Meroufel, F. Al Muaili, Case Studies in Engineering Failure Analysis 3 (2015) 96-103.
[19] R. Saluja, K. M. Moeed, Int. J. Eng. Sci. Technol. 4 (2012) 2206-2212.
[20] E. J. Barnhouse, J. C. Lippold, Weld. J. 77 (1998) 477-484.
[21] S. Kumar, A. S. Shahi, Mater. Des. 32 (2011) 3617-3624.
[22] R. Yilmaz, H. Uzun, Journal of Marmara of Pure and Applied Sciences 18 (2002) 97.